Research Article | Vol. 26, No. 18 | 3 Sep 2018 | OPTICS EXPRESS 23196
Optics EXPRESS

Nonlinear propagation and quasi self-confinement of light in plasmonic resonant media

VLADLEN SHVEDOV,[1] KONRAD CYPRYCH,[2,3] M. YADIRA SALAZAR-ROMERO,[1,4] YANA IZDEBSKAYA AND WIESLAW KROLIKOWSKI[1,2,*]

[1]*Laser Physics Centre, Research School of Physics and Engineering, Australian National University, Canberra, ACT 0200, Australia*
[2]*Science Program, Texas A&M University at Qatar, Doha, Qatar*
[3]*Advanced Materials Engineering and Modelling Group, Wroclaw University of Science and Technology, Wroclaw, Poland*
[4]*Instituto de Física, Universidad Nacional Autónoma de México, Apdo. Postal 20-364, Mexico, D.F., Mexico*
[*]*wieslaw.krolikowski@anu.edu.au*

Abstract: We study nonlinear propagation of light in colloidal suspension of metallic nanoparticles, in the regime of particles surface plasmon resonance. We show that the propagation exhibits features typical for purely defocusing media and the observed spatial confinement is not a real self-trapping, as for solitons, but rather than is caused by the phase modulation of the beam via nonlocal defocusing nonlinearity. We also show that the light-induced refractive index change in the suspension leads to stabilization of structured light beams. In particular, we demonstrate a stable nonlinear propagation of bright ring beams with complex states of polarization, including practically important radial and azimuthal states.

OCIS codes: (190.4420) Nonlinear optics; (160.4236) Nanomaterials; (240.6680) Surface plasmons; (050.4865) Optical vortices.

References and links

1. A. S. Reyna, K. C. Jorge, and C. B. de Araújo, "Two-dimensional solitons in a quintic-septimal medium," Phys. Rev. A **90**, 063835 (2014).
2. A. S. Reyna and C. B. De Araujo, "Guiding and confinement of light induced by optical vortex solitons in a cubic–quintic medium," Opt. Lett. **41**, 191–194 (2016).
3. P. Reece, E. Wright, and K. Dholakia, "Experimental observation of modulation instability and optical spatial soliton arrays in soft condensed matter," Phys. Rev. Lett. **98**, 203902 (2007).
4. R. El-Ganainy, D. Christodoulides, C. Rotschild, and M. Segev, "Soliton dynamics and self-induced transparency in nonlinear nanosuspensions," Opt. Express **15**, 10207–10218 (2007).
5. T. S. Kelly, Y.-X. Ren, A. Samadi, A. Bezryadina, D. Christodoulides, and Z. Chen, "Guiding and nonlinear coupling of light in plasmonic nanosuspensions," Opt. Lett. **41**, 3817–3820 (2016).
6. W. Man, S. Fardad, Z. Zhang, J. Prakash, M. Lau, P. Zhang, M. Heinrich, D. N. Christodoulides, and Z. Chen, "Optical nonlinearities and enhanced light transmission in soft-matter systems with tunable polarizabilities," Phys. Rev. Lett. **111**, 218302 (2013).
7. W. Lee, R. El-Ganainy, D. Christodoulides, K. Dholakia, and E. Wright, "Nonlinear optical response of colloidal suspensions," Opt. Express **17**, 10277–10289 (2009).
8. W. Walasik, S. Z. Silahli, and N. M. Litchinitser, "Dynamics of necklace beams in nonlinear colloidal suspensions," Sci. Rep. **7**, 11709 (2017).
9. M. Matuszewski, W. Krolikowski, and Y. S. Kivshar, "Spatial solitons and light-induced instabilities in colloidal media," Opt. Express **16**, 1371–1376 (2008).
10. C. F. Bohren and D. R. Huffman, *Absorption and scattering of light by small particles* (John Wiley & Sons, 2008).
11. V. Amendola, R. Pilot, M. Frasconi, O. M. Maragò, and M. A. Iatì, "Surface plasmon resonance in gold nanoparticles: a review," J. Phys.: Condens. Matter **29**, 203002 (2017).
12. J. Olson, S. Dominguez-Medina, A. Hoggard, L.-Y. Wang, W.-S. Chang, and S. Link, "Optical characterization of single plasmonic nanoparticles," Chem. Soc. Rev. **44**, 40–57 (2015).

#336145 https://doi.org/10.1364/OE.26.023196
Journal © 2018 Received 27 Jun 2018; revised 8 Aug 2018; accepted 8 Aug 2018; published 24 Aug 2018

Optics EXPRESS

13. H. Chen, X. Kou, Z. Yang, W. Ni, and J. Wang, "Shape-and size-dependent refractive index sensitivity of gold nanoparticles," Langmuir **24**, 5233–5237 (2008).
14. S. Lal, S. Link, and N. J. Halas, "Nano-optics from sensing to waveguiding," Nat. Photonics **1**, 641 (2007).
15. J. N. Anker, W. P. Hall, O. Lyandres, N. C. Shah, J. Zhao, and R. P. Van Duyne, "Biosensing with plasmonic nanosensors," Nat. Mater. **7**, 442 (2008).
16. S. Fardad, A. Salandrino, M. Heinrich, P. Zhang, Z. Chen, and D. N. Christodoulides, "Plasmonic resonant solitons in metallic nanosuspensions," Nano Lett. **14**, 2498–2504 (2014).
17. K. Svoboda and S. M. Block, "Optical trapping of metallic Rayleigh particles," Opt. Lett. **19**, 930–932 (1994).
18. S. IIto, H. Yamauchi, M. Tamura, S. Hidaka, H. Hattori, T. Hamada, K. Nishida, S. Tokonami, T. Itoh, H. Miyasaka, and T. Iida, "Selective optical assembly of highly uniform nanoparticles by doughnut-shaped beams," Sci. Rep. **3**, 3047 (2013).
19. Y. Seol, A. E. Carpenter, and T. T. Perkins, "Gold nanoparticles: enhanced optical trapping and sensitivity coupled with significant heating," Opt. Lett. **31**, 2429–2431 (2006).
20. P. M. Hansen, V. K. Bhatia, N. Harrit, and L. Oddershede, "Expanding the optical trapping range of gold nanoparticles," Nano Lett. **5**, 1937–1942 (2005).
21. C. Selhuber-Unkel, I. Zins, O. Schubert, C. Sonnichsen, and L. B. Oddershede, "Quantitative optical trapping of single gold nanorods," Nano Lett. **8**, 2998–3003 (2008).
22. P. Schiebener, J. Straub, J. Levelt Sengers, and J. Gallagher, "Refractive index of water and steam as function of wavelength, temperature and density," J. Phys. Chem. Ref. Data **19**, 677–717 (1990).
23. A. S. Desyatnikov, L. Torner, and Y. S. Kivshar, "Optical vortices and vortex solitons," Prog. Opt. **47**, 291–391 (2005).
24. Y. V. Kartashov, V. A. Vysloukh, and L. Torner, "Stabilization of higher-order vortices and multihump solitons in media with synthetic nonlocal nonlinearities," Phys. Rev. A **79**, 013803 (2009).
25. Y. V. Kartashov, V. A. Vysloukh, and L. Torner, "Engineering soliton nonlinearities: from local to strongly nonlocal," Opt. Lett. **34**, 1543–1545 (2009).
26. M. Shen, B. Li, L. Ge, W. Chen, and D. Wu, "Stability of vortex solitons under competing local and nonlocal cubic nonlinearities," Opt. Commun. **338**, 27–33 (2015).
27. E. Brasselet, Y. Izdebskaya, V. Shvedov, A. S. Desyatnikov, W. Krolikowski, and Y. S. Kivshar, "Dynamics of optical spin-orbit coupling in uniaxial crystals," Opt. Lett. **34**, 1021–1023 (2009).
28. Q. Zhan and J. R. Leger, "Focus shaping using cylindrical vector beams," Opt. Express **10**, 324–331 (2002).
29. R. F. Souza, M. A. R. C. Alencar, E. C. da Silva, M. R. Meneghetti, and J. M. Hickmann, "Nonlinear optical properties of au nanoparticles colloidal system: Local and nonlocal responses," Appl. Phys. Lett. **92**, 201902 (2008).
30. L. Novotny, M. Beversluis, K. Youngworth, and T. Brown, "Longitudinal field modes probed by single molecules," Phys. Rev. Lett. **86**, 5251 (2001).
31. K. Watanabe, N. Horiguchi, and H. Kano, "Optimized measurement probe of the localized surface plasmon microscope by using radially polarized illumination," Appl. Opt. **46**, 4985–4990 (2007).
32. E. Yew and C. Sheppard, "Second harmonic generation polarization microscopy with tightly focused linearly and radially polarized beams," Opt. Commun. **275**, 453–457 (2007).
33. N. Hayazawa, Y. Saito, and S. Kawata, "Detection and characterization of longitudinal field for tip-enhanced Raman spectroscopy," Appl. Phys. Lett. **85**, 6239–6241 (2004).
34. C. Hnatovsky, V. Shvedov, W. Krolikowski, and A. Rode, "Revealing local field structure of focused ultrashort pulses," Phys. Rev. Lett. **106**, 123901 (2011).
35. D. Biss and T. Brown, "Polarization-vortex-driven second-harmonic generation," Opt. Lett. **28**, 923–925 (2003).
36. Q. Zhan, "Trapping metallic rayleigh particles with radial polarization," Opt. Express **12**, 3377–3382 (2004).
37. V. Shvedov, A. R. Davoyan, C. Hnatovsky, N. Engheta, and W. Krolikowski, "A long-range polarization-controlled optical tractor beam," Nat. Photonics **8**, 846–850 (2014).
38. Y. S. Kivshar and G. Agrawal, *Optical solitons: from fibers to photonic crystals* (Academic Press, 2003).

1. Introduction

Suspensions of nanoparticles have attracted great interest in the field of light-matter interaction due to their abilities to confine light beams and form solitons in both, short pulse [1, 2] and continuum wave (cw) regimes [3–9]. In the latter case the metallic nanoparticles are of particular interest because of their unique optical properties exhibiting surface plasmon resonance [7, 10–12]. The interaction with electromagnetic radiation depends strongly on the wavelength and polarization of light as well as on size and shape of particles [5, 6, 13–16]. The tailored combination of these parameters can dramatically affect optical properties of a suspension, typically in small focal volume of a tightly focused laser beam, by assembling particles via optical trapping [17, 18]. Recently, it was proposed [5, 16] that suspensions of gold nanoparticles illuminated with light of frequency near their surface plasmon resonance may change the local concentration of

Optics EXPRESS

nanoparticles along a low-divergence beam by action of the polarizability-dependent gradient force acting on the particles. This leads to the modulation of the refractive index of the suspension within the beam, supporting nonlinear self-guiding of the latter. For low light intensity, the suspension behaves as linear medium with an average refractive index determined by the concentration of nanoparticles. On the other hand, in case of illumination by an intense laser beam, both gradient force and light absorption change the refractive index of the suspensions around the beam in different ways. The change of concentration of particles by the action of gradient force increases refractive index of the suspensions in the beam center, while light induced non-local thermal response of the surrounding liquid leads to decreasing of the refractive index within and outside of the beam [19]. The joint action of these processes may ensure net increase of refractive index leading to the self-confinement of the incident beams at a long distance in the form of spatial solitons [1, 2, 4, 16] and their subsequent ability to guide optical signals at nonresonant wavelengths [5].

In this work we study in great detail propagation of optical beams in metallic suspensions. In particular, we look at the possibility of low-divergent beams to change locally the concentration of nanoparticles and subsequently, increase the refractive index of plasmonic aqueous suspensions by means of optical forces. We show that thermo-optical response is, in fact, a dominating process preventing the refractive index increase and, hence, making the true self-trapping of the beams practically impossible. The experimentally observed apparent "self-focusing" of the beam is caused by the modulation of wavefront of the beam by spatially nonlocal defocusing nonlinearity.

2. Gradient force

Let us start from an estimation of the gradient force acting on gold nanospheres in aqueous suspension, illuminated by a low-divergence monochromatic Gaussian beams including also ring-shaped beams. The latter condition means that $w_0 >> \lambda_0$, where w_0 is the beam waist radius and λ_0 is the wavelength of the beam in vacuum. The gradient force for an isotropic particle is given as $\mathbf{F}_{grad} = (1/4)\alpha_R \nabla \{\mathbf{E}(r) \cdot \mathbf{E}^*(r)\}$, where complex function $\mathbf{E(r)}$ represents the electric field $\mathbf{E}(\mathbf{r}, t) = \mathbf{E}(\mathbf{r})e^{i(kz-\omega t)}$ of monochromatic light and α_R is the real part of the particle's polarizability $\alpha = 4\pi\varepsilon_0 a^3(\varepsilon_g - \varepsilon_w)/(\varepsilon_g + 2\varepsilon_w)$ [10]. Here ε_0 is the dielectric permittivity of vacuum, ε_g is the frequency-dependent permittivity of the gold nanosphere of radius a, and ε_w is the permittivity of surrounding water.

In the linear (low power) regime of propagation, we assume the intensity profile of Gaussian beams to be $I^{(m)}(\rho, z) = P\rho^{2m}e^{-\rho^2/w^2(z)}/\pi m! w(z)^{2(m+1)}$, where P is a beam power, $m = 0, 1..$, $w(z) = w_0(1 + z^2/z_0^2)^{1/2}$ is the beam radius coinciding with the radius of the maximum intensity contour of the beam with $m = 1$, $z_0 = k_w w_0^2$ is a parameter characterizing the beam divergence, and $k_w = 2\pi n_w/\lambda_0$ denotes the wave number. For the zero-order Gaussian beam ($m = 0$), the maximum gradient force is then $F_{grad}^{max} = Pn_w\alpha_R\sqrt{2e}/(2\pi c\varepsilon_0 w_0^3)$, where c refers to speed of light. Let the wavelength of the beam in vacuum be $\lambda_0 = 532$ nm, and the radius of gold nanospheres be $r_p = 20$ nm with the peak of absorption at $\lambda_r = 524$ nm. The permittivity of the nanosphere at $\lambda_0 = 532$ nm is $\varepsilon_g = -4.68 + 2.43i$ and the dielectric constant of water $\varepsilon_w = n_w^2 = 1.33^2$ at $20°C$. For the beam waist of w_0=10 μm, we find that $F_{grad}^{max}/P \approx 3 \times 10^{-4}$ pN/W. Note that the maximum gradient force for a ring-shaped beam of the same power is even lower. For instance for the beam with $m = 1$ this force is 1.5 and 2.2 times less for the direction to and out of the contour of the ring, respectively. Under the action of the gradient force, a particle acquires a speed of $v_p = \mu F_{grad}$ towards the intensity maximum, where μ is the particle's mobility in water. The mobility for a spherical particle is $\mu = 1/6\pi\eta a$, where $\eta = 1$ mPa·s is the dynamic viscosity of water at 20° C. Thus, the 20-nm-radius gold nanosphere may drift by action of the gradient force in the optical beam of 100 mW power with an estimated maximal speed about $v_g \approx 10^{-6}$ m/s. This is incredibly low speed which is five orders of magnitude slower than the root mean square velocity of Brownian motion of the nanosphere ($\langle v_b \rangle \approx 0.13$ m/s).

Optics EXPRESS

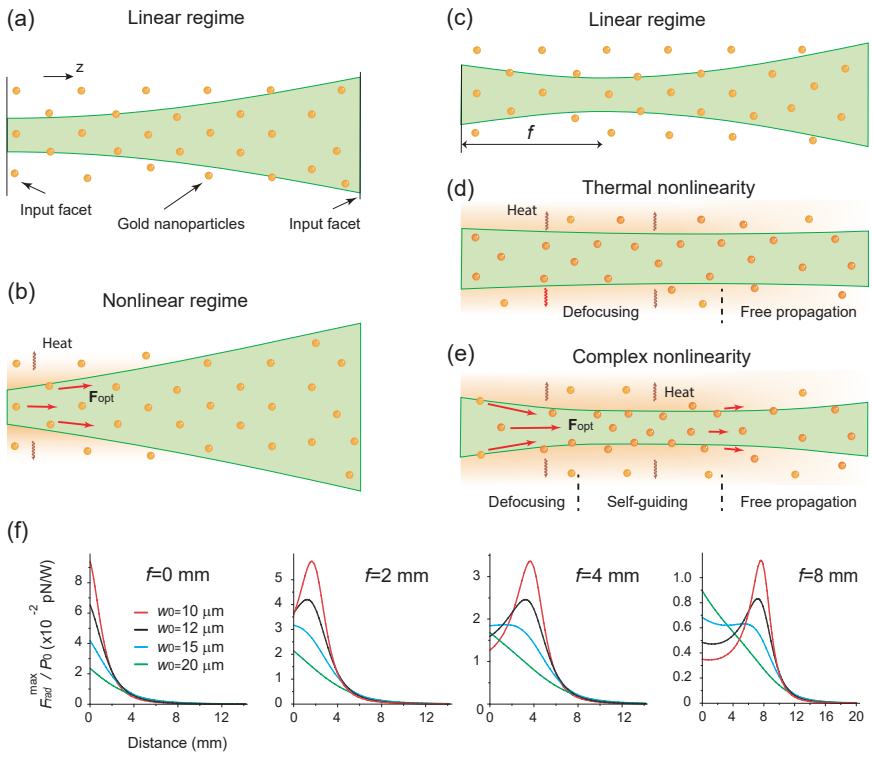

Fig. 1. Illustration of the beam propagation concept in the aqueous suspension of gold nanospheres. (a),(b) the beam propagation in a linear (a) and nonlinear (b) regimes when its waist is at the input facet of the cell with the suspension. The low light power has no effects on the random particle distribution in the suspension (a). Increasing the beam power leads to the decreasing of the refractive index of the suspension caused by the negative thermo-optical response of water (orange zone) (b). The probable optical force increases the defocusing effect. (c), (d) The beam propagation in a linear (c) and nonlinear (d, e) regimes when its waist is inside the suspension. In the nonlinear regime (d) the optical forces play no role and the heated water lowers the refractive index of the suspension defocusing the beam and, as result, the actual beam waist increases lowering the beam divergence. In the nonlinear regime (e) the optical forces may locally increase the concentration of particles near the focus creating both positive nonlinearity with high local refractive index in the beam maximum and negative nonlocal thermal optical response with a low refractive index of the surrounding liquid (orange region). The competition between these nonlinear processes may potentially lead to the self-guiding of the beam. (f) Calculated maximal radiation force acting on gold nanospheres as a function of beam waist w_0 and a position of the focus (f) measured from the front facet of the cell. The absorption coefficient of the suspension is assumed to be $\eta = 0.27 \times 10^3\ m^{-1}$.

Optics EXPRESS

3. Radiation force

Besides the gradient force the total optical force acting on a gold nanoparticle contains two other contributions: the absorption forces $\mathbf{F}_{abs} = n_w \langle \mathbf{S} \rangle C_{abs}/c$ and the scattering force $\mathbf{F}_{scat} = n_w \langle \mathbf{S} \rangle C_{scat}/c$. Here $\langle \mathbf{S} \rangle$ is the time-averaged Poynting vector, $C_{abs} = k_w \mathrm{Im}(\alpha)/\varepsilon_0$ and $C_{scat} = k_w^4 |\alpha|^2 / 6\pi\varepsilon_0^2$ are the absorption and scattering cross sections, respectively. While the gradient force tends to agglomerate nanoparticles, both the absorption and scattering force tend to destabilize this tendency by pushing the particles in the direction of the light energy flux [17]. Using the same parameters as above, we find the maximum absorption force $F_{abs}^{max}/P \approx 4 \cdot 10^{-2}$ pN/W, and the maximum scattering force $F_{scat}^{max}/P \approx 10^{-2}$ pN/W. The speed that a particle acquires by the action of these forces is about $v_a \approx 10^{-4}$ m/s. This estimation shows that in the example the joint action of repulsive optical forces (radiation force) is two orders of magnitude stronger than the gradient force, and thus, the latter should play no significant role in the nonlinear light-matter interaction with low-divergence optical beams. In other words, the repulsive radiation force highly dominates over the gradient force and is mainly responsible for the total action of the optical force in the plasmonic suspension. It should be emphasized that our interest here lies in a nonlinear response of nanosuspension induced by low-divergence optical beams. In tightly focusing laser beams ($w_0 \approx \lambda_0$), the action of the gradient force may exceed the radiation force leading to a stable trapping of a single or multiple metallic nanoparticles [17, 18, 20, 21]. However, the trapping region in this case is limited to the tiny focal spot comparable with a wavelength of light and cannot dramatically impact on the nonlinear properties of the suspension.

4. Thermo-optical response of plasmonic nanosuspensions

The other relevant process affecting the light interaction with metallic suspension is thermo-optical response of the suspension to the incident light. The particles absorb a large fraction of the incident light generating heat which is subsequently transferred to the surrounding water. The speed of a single particle heating is $v_p = 2a/t_p$, where $t_p = a^2/\kappa_g$ is a time of the heat diffusion, and $\kappa_g = 1.27 \cdot 10^{-4} m^2/s$ is diffusivity of gold. The subsequent heating speed of water is $v_w = l/t_w$, where l is a distance between particles, $t_w = l^2/2\kappa_w$ is a time of water heating, $\kappa_w = 0.43 \cdot 10^{-6} m^2/s$ is diffusivity of water. The suspension of discussed here gold nanospheres with concentration of 0.05 mg/mL gives heating time (speed) of $t_p = 3.5 \times 10^{-12}$s ($v_p$=$10^4$m/s) and t_w=10^{-6}s (v_w=1m/s) for gold nanospheres and water, respectively. The heating of water stimulates the temperature-dependent refractive index change which can be approximated by $\Delta n_T = (\partial n_b/\partial T)(T - T_b)(1 - f_V)$, where T represents spatial temperature distribution and T_b is the initial temperature of the suspension and f_V is the volume filling fraction of nanoparticles. The thermo-optic coefficient $\partial n_b/\partial T$ of a suspension with low concentration of particles ($f_V << 1$) is negative as it is predominantly determined by that of water [16] which is $\partial \mathrm{n}_b/\partial T \approx -10^{-4} K^{-1}$ [22]. With the temperature increase a background refractive index, n_b, decreases leading to the negative (defocusing) thermal nonlinearity which is inherently spatially nonlocal because of heat diffusion.

5. Position-dependent scenario of light-matter interaction

According to our above estimations, the heating process is much faster than the process of particle transport by the optical forces. Therefore, the heated water induces a quasi-stationary background of spatially-dependent refractive index distribution defining nonlinear optical response of the colloidal nanosuspension. The radiation force acting on particles may also potentially play a role in the redistribution of the refractive index via a local change of particles concentration. If this happens, it should lead to a specific nonlinear behavior of propagating beams. Figure 1 shows the expected behavior of light, considering, as an example, a low-divergence Gaussian beams focused at the front facet Figs. 1(a) and 1(b) or inside Figs. 1(c)-1(e) of the cell with gold nanosuspension. In the low-power regime of propagation in both cases, the beam just diffracts linearly losing its

Optics EXPRESS

power as $P = P_0 e^{(-\eta z)}$, where P_0 is the initial power and η is the absorption coefficient of the suspension. Nevertheless, in a high-power regime, the nonlinear beam behavior may critically depend on position of the beam waist in the suspension. When the waist position is located before or at the boundary of the cell, the increasing power leads to the strong thermo-optical response of water, defocusing the beam. In this situation the optical force rapidly vanishes with the distance of propagation z due to both the beam diffraction and absorption (see the first graph in Fig. 1(f)). Moreover, the optical force can only contribute to the defocusing process, at least for particles with positive polarizability. Whereas the gradient force is too weak to counteract rapid thermal motion of nanoparticles and attract them to the beam center, both the absorption and scattering forces tend to push particles out of the focal spot preventing their agglomeration.

The situation may change when the beam is focused deep inside the suspension. The radiation force acting on nanoparticles can now be defined as $\mathbf{F}_{rad} \approx P_0 e^{-\eta z} \mathrm{Im}(\alpha) \mathbf{k}_w / \varepsilon_0 c w_0^2 (1 + (z - f)^2 / z_0^2)$, where $\mathbf{k}_w$ is the wave vector and f is a distance from the input to the position of the beam waist. Depending on the size and position of the beam waist, the radiation force may change significantly in the vicinity of focal area increasing before and decreasing after the focus (see Fig. 1(f)). Under this force the particles move to the focal area along the energy flux and, in an ideal scenario of absence of a significant thermal motion of particles, may potentially increase their local concentration. This situation is schematically shown in Fig. 1(e). While the thermo-optical response of the suspension decreases exponentially with the distance z, the increased concentration of particles will locally elevate the refractive index at the beam axis near the focal position. Such a zone may potentially support the self-confinement of optical beam over a short distance of optimal balance between thermal defocusing and concentration-dependent self-focusing in the suspension (self-guiding zone in Fig. 1(e)). After the focal plane though, the optical force repels the assembly of particles, preventing further self-confinement.

In the above discussion we have assumed that the size and position of the focal spot is unchanged when the power increases. However, in an realistic scenario of focusing a beam inside the suspension, the nonlinear properties far before the focal spot are mostly defined by the thermo-optical response of heated water as the optical force plays no significant role in the redistribution of particles concentration there. This creates only defocusing nonlinearity with lower refractive index along the beam propagation and results in changing the beam divergence (see defocusing zone in Fig. 1(d)). In other words, the diffraction length of the beam is expected to increase within certain range of the power growth, resulting in the apparent beam self-confinement. This defocusing process weakens gradually along z because of light absorption, and after that the quasi linear diffraction will take place (free propagation zone in the Fig. 1(d)). Note that in such a process, the optical forces should have no influences on the homogeneous particle distribution as well as on the refractive index of the suspension. The two scenarios considered above predict almost identical behavior of an output optical beam as a function of its power and the initial focal position inside the suspension. Indeed, the size of the beam at the output facet of the cuvette may show a similar tendency as a function of input power (see Figs. 1(d) and 1(e)). Moreover, the nonlinear transformation of the beam may support apparent guiding of the co-propagating beams at different wavelength. Nevertheless, the actual formation of a true self-guiding requires refractive index increase at the beam axis. This, in turn, should lead to nonlinear absorption (due to larger particle concentration) of the beam and strongly affect stability of the higher order beams.

6. Experiment

To clarify the light-matter interaction in metallic colloids we conducted series of experiments with fundamental and ring-shaped Gaussian optical beams. In the first instance, we studied nonlinear behavior of the fundamental Gaussian beam (wavelength 532 nm in vacuum) with fixed position of the beam waist w_0=7.5 μm at the distance of 5.7 mm from the input of the 20

Optics EXPRESS

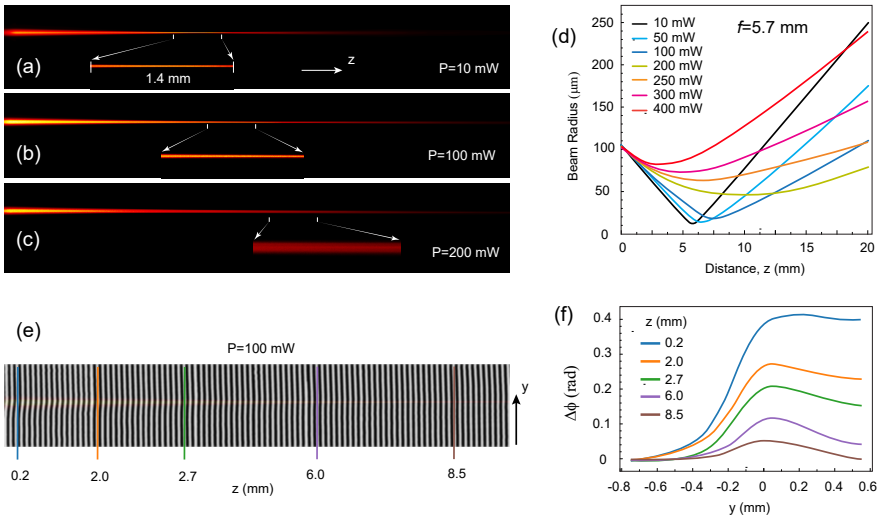

Fig. 2. Side-view observation of Gaussian beam propagation in suspension of 20-nm-radius gold nanospheres with absorption coefficient η=0.133 m^{-1}. (a-c) Evolution of the beam radius with power. Insets show magnified sections around beam waist. (d) Measured width of the beam at the output versus input power. (e) Distortion of interference fringes and corresponding inhomogeneous phase shift (f) induced by the beam.

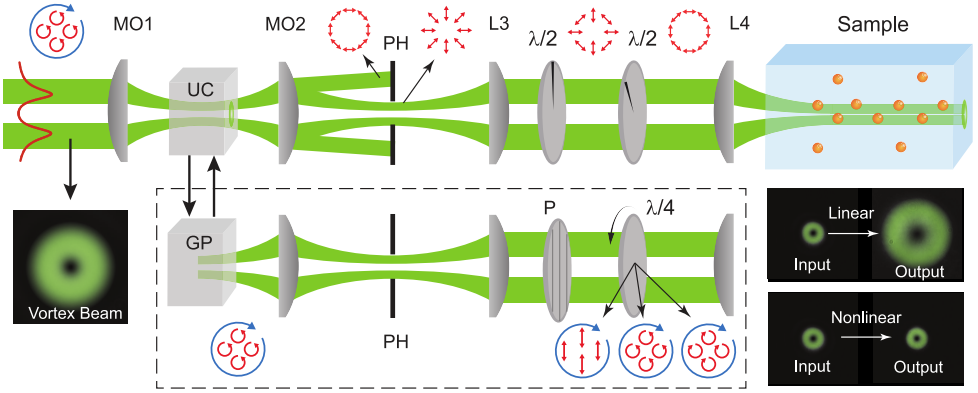

Fig. 3. Schematic diagram of the experimental setup for the beam convertor and ring beam formation. In the upper row, the uniaxial crystal (UC), microobjectives MO1 and MO2, pinhole PH and lens L3 are used to separate the radially polarized beam from a circularly polarized vortex. Blue arrows show the direction of a vortex rotation; red arrows show the states of polarization. The polarizer, half-wave plates and quarter-wave plates used to change the polarization state of the beam are denoted by P, $\lambda/2$ and $\lambda/4$, respectively. In the lower row, the crystal is replaced with a glass prism GP with the same optical length to give a free pass to the initial optical vortex. The lenses L3 and L4 are used to collimate and focus a beam to the sample. Examples of the radially polarized beam at the input and output facets in linear (1 mW) and nonlinear (80 mW) regimes are shown in black pictures.

Optics EXPRESS

mm long cuvette which was filled with aqueous suspension of gold nanospheres (diameter 40 nm, concentration 0.05 mg/mL). The light intensity distribution and the refractive index change of the suspension were monitored at the transparent side facets of the cuvette by collecting the scattered light with an optical microscope. Results of these experiments are depicted in Fig. 2. For the power range from 10 mW to 200 mW, the beam waist tends to spread and move forwards with increasing power. The side-view pictures in Figs. 2(a)-2(c) shows this tendency for three different input powers. The insets depict the increasing of the beam waist, thereby decreasing its divergence. As a result, the size of the output beam is smaller for higher power in that range. The graphs in Fig. 2(d) depict the power-dependent evolution of the beam width with a distance. One can clearly see that for the power level around 200 mW the beam exhibits relatively low divergence over quite significant distance which appears as apparent self-confinement. However, this effect is caused by nonlocal defocusing of thermal origin. This is further confirmed in interference experiment, in which cuvette with the propagating beam was inserted into a one arm of Mach-Zehnder interferometer. The corresponding interference pattern obtained with red (721nm) light and the extracted phase change across the beam at various position within the cuvette are shown in Figs. 2(e) and 2(g). The shift of fringes in the beam area and above it (due to heat convection) with negative phase change around the beam axis indicates the decreasing of the refractive index reflecting defocusing response.

In the subsequent experiments we investigated the nonlinear behavior of beams with complex intensity, phase and polarization using, as example, ring-shaped beams. If the local self-focusing takes place in the suspension, the ring-shaped beams should be a subject of destructive amplitude and phase perturbations leading to the azimuthal instability [8,23]. On the other hand, nonlocality of the negative refractive index change provided only by the thermo-optical response typically supports stable complex structure beam in nonlinear defocusing media [24–26]. Therefore one may expect that a beam with complex intensity and polarization structure should break into individual filaments in the local self-focusing media or preserve their structure in the non-local defocusing media. To be consistent, in our experiments we generated all ring-shaped beams with a single setup as shown in Fig. 3. In particular, all the beams were derived from the initial circularly polarized single charge optical vortex by straightforward polarization transformations. The electric field of such a beam $\mathbf{E}^- = E(\rho, z)e^{i\varphi}\boldsymbol{\sigma}^-$ can be represented as a superposition of electric fields of radially and azimuthally polarized beams: $\mathbf{E}^- = (\mathbf{E}_\rho - i\mathbf{E}_\varphi)/\sqrt{2}$. The vortex was propagating along the optical axis of 10-mm-long c-cut calcite crystal placed between two identical microscope objectives MO1 and MO2 (NA=0.25). As both radially and azimuthally polarized beams are eigenmodes of a uniaxial crystal [27] with different divergences, their waists were axially separated after the crystal at the distance ~ 1.5 mm with respect to each other. The circular pinhole with the radius 50 μm was placed in the waist plane of the radially polarized beam so that the azimuthally polarized component was removed and did not contribute to the the final polarization state. After the pinhole the resulting radially polarized beam was collimated and could be converted to other types of the singular beams with complex polarization, before focusing. The antivortex beam was derived from the radially polarized beam by straightforward polarization transformations with a first half waveplate after the pinhole as it is shown in the upper row of the Fig. 3. By placing and rotating the second half-wave plate, one can change the polarization state of the antivortex beam to the azimuthal or radial without affecting its other parameters [28]. Thus, these three vector beams had identical initial intensity distributions. Vortex beams of different polarizations was derived from the initial circularly polarized vortex beam in the same forming setup but with the calcite crystal replaced with 10-mm-long glass prism (see the bottom row in Fig. 3). The conversion between different states of polarization was obtained with a polarizer and a quarter waveplate located after the pinhole. Thus, the resulting vortex beams have identical to vector beams intensity distributions. This allowed the beams to maintain the same conditions in a linear regime of propagation. All the ring-shaped beams had beam

Optics EXPRESS

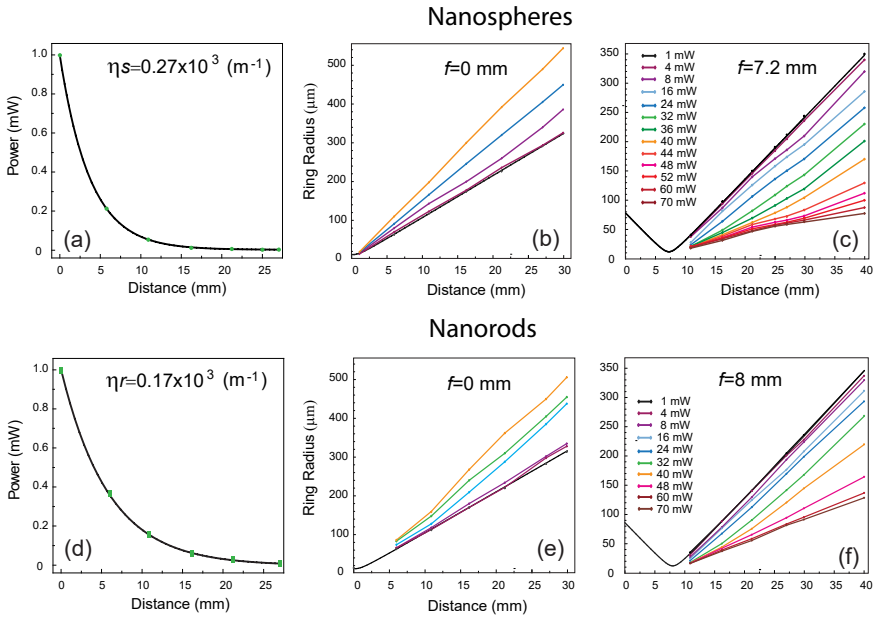

Fig. 4. Results of the nonlinear propagation of ring-shaped beams in suspension of gold nanospheres (a-c) and gold nanorods (d-f). (a), (d) Measured power absorption of the suspensions. (b,c) and (e,f) Radius of the ring-shaped beams at the output facet of cuvettes as a function of the initial beam power and position of the beam waist for the nanospheres and nanorods, respectively. Dots represent experimental data while lines are averaged fits.

width $w(z) = w_0\sqrt{1+(z-l)^2/z_0^2}$ with the same position of the beam waist w_0=12 μm inside the cuvette in linear regime of propagation. The set of considered beams included four types of high-order beams with the same ring-shaped intensity distributions: x-polarized single charge m=1 optical vortex with complex amplitude of the electric field $\mathbf{E}_x = E^{(1)}(\mathbf{r})e^{i\varphi}\mathbf{e}_x$; circularly polarized vortex with the same signs of handedness σ=1 and chirality m=1: $\mathbf{E}^+ = E^{(1)}(\mathbf{r})e^{i\varphi}\boldsymbol{\sigma}^+$; as well as radially polarized $\mathbf{E}_\rho = E^{(1)}(\mathbf{r})\mathbf{e}_\rho$ and azimuthally polarized $\mathbf{E}_\varphi = E^{(1)}(\mathbf{r})e_\varphi$ beams. Here $E^{(m)} = \sqrt{2I^{(m)}}/cn_w\varepsilon_0$, $\boldsymbol{\sigma}^\pm\sqrt{2} = (\mathbf{e}_x \pm i\,\mathbf{e}_y) = (\mathbf{e}_\rho \pm i\,\mathbf{e}_\varphi)e^{\pm i\varphi}$ is a unit vector corresponding to right (+) and left (-) hand polarization; $\mathbf{e}_x$, $\mathbf{e}_y$, $\mathbf{e}_z$ and $\mathbf{e}_\rho$, $\mathbf{e}_\varphi$ denote unit vectors in Cartesian and polar coordinates, respectively. Thus, all ring-shaped beams had the same initial intensity distribution $I^{(1)}(\rho,z) = P\rho^2 e^{-\rho^2/w(z)^2}/\pi w(z)^4$.

In the experiment we used two identical sets of glass cuvettes with various lengths of 1, 6, 10.9, 16.2, 21.2, 25, 27, 30, and 40 mm. We monitored the nonlinear transformation of beam intensities as a function of power and propagation distance. In one series of experiments the cuvettes were filled with the suspension of gold nanospheres as in experiment above, while in the second one, with the suspension of gold nanorods (width 50 nm, length 100 nm). The experiments with nanorods aimed checking a possible nonlinear dependence of the propagation on a polarization structure of the incident beam via orientational nonlinearity. The position of the beam waist inside the cuvettes was controlled with the micro-translation stage and the input power of the beam was adjusted with a gradient transmission filter.

At low power, P < 1 mW, each beam propagates linearly, and their ring radius expands due to diffraction (see black curves in the Fig. 4). The similar smooth transition from the linear to the nonlinear propagation was observed in both suspensions with gradually increasing power. The spatial evaluation of beam radius at various input power levels and initial waist positions is

Optics EXPRESS

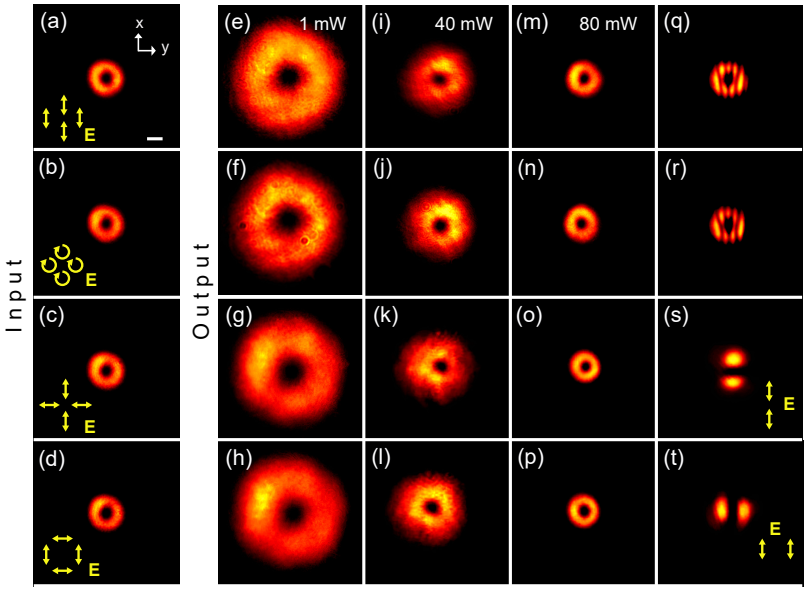

Fig. 5. Observation of stable nonlinear propagation of ring-shaped beams in the suspension of gold nanospheres. Each beam of identical intensity distributions was initially focused inside the cell, 6 mm from its front facet. (a)-(d) Input and (e)-(t) output profiles for a linearly polarized vortex (first row), circularly polarized vortex (second row), radially (third row) and azimuthally polarized vector (fourth row) beams. Yellow arrows indicate the state of polarization. (e)-(p) Output beam profiles after 2.5 cm of propagation at different input power levels, showing the transition from diffractive broadening at 1 mW to nonlinear narrowing at 80 mW. (q), (r) The interferograms confirming the vortex nature. (s), (t) Intensity distributions of radially and azimuthally polarized beams after an analyzer. The scale bar in (a) corresponds to 500 μm.

depicted using different colors in the graphs of Fig. 4. The narrowing, intensity and polarization distributions of the beams at various input power levels as they are focused at the distance of 6 mm in 25-length cuvette filled with gold nanospheres are depicted in Fig. 5. We observe that all the ring-shaped beams maintain their intensity profile and polarization structure throughout the nonlinear transformation at the power range up to 90 mW. For higher input power, the size of rings increases and the beams gradually lose their perfect symmetry due to the thermal convection but without any break-up into filaments. Interestingly, the beam size is extremely sensitive to the power variations even at very low power of a few mW indicating that the thermal nonlinear processes already start at this power level.

7. Conclusions

These observations confirmed that the quasi diffraction-free propagation of the high intensity beam in plasmonic nano-suspension was not caused by the self-trapping but the phase modulation via nonlocal refractive index decrease (self-defocusing). Furthermore, we found complete lack of nonlinear absorptions in all our experiments irrespectively of the beam power and beam waist positions in the suspensions. This indicates no changes in particle concentrations in the nonlinear process. These observations are consistent with previously reported absence of nonlinear absorption in metallic nanosuspensions [29].

It is also worth to mention, that we found no principal differences in the beam behavior in both nanospheres and nanorods colloids except for power range needed to observe the nonlinear

Optics EXPRESS

processes (because of different absorption). This indicates that also in the suspension of nanorods, the thermal nonlinearity induced by the light absorption significantly dominates over the possible orientational nonlinearity caused by optical torque.

Despite the fact that our measurements show only the thermally-dependent nonlinearity of the suspensions for low-divergence optical beams, the stable propagation of the ring-shaped beams in nonlinear regime is still an important result. The refractive index change provided by the thermo-optical response of a plasmonic nanosuspension suppresses typical azimuthal instabilities inherent to focusing nonlinear media, supporting stable propagation of beams with complex intensity and polarization distributions. The intensity distribution and state of light polarization are crucial parameters for any photonic technique requiring precise control of light-matter interaction. While the structured light is now routinely used in various applications including high resolution microscopy [30–32], Raman spectroscopy [33], material processing [34], second harmonic generation [35], particle trapping and manipulation [36, 37], their use in nonlinear optical media is scarce [7] because complex beams are typically susceptible to structural instabilities in propagation [38]. We believe that the demonstrated here structural stability of complex beams in plasmonic nanosuspensions unveils potentially rich scenarios for nonlinear-based optical circuits and reconfigurable photonic interconnects.

Funding

Qatar National Research Fund (grant # NPRP 9-020-1-006). Y.S-R. acknowledges support from CONACyT and Australian and Mexican Academies of Science for Ph.D. internship grant.